CONFIDENTIAL

NACA RM H56A23

NACA

RESEARCH MEMORANDUM

FLIGHT MEASUREMENTS OF HORIZONTAL-TAIL LOADS ON THE DOUGLAS X-3 RESEARCH AIRPLANE

By Harriet J. Stephenson

High-Speed Flight Station
Edwards, Calif.

NATIONAL ADVISORY COMMITTEE
FOR AERONAUTICS

WASHINGTON

April 18, 1956

CONFIDENTIAL

NATIONAL ADVISORY COMMITTEE FOR AERONAUTICS

RESEARCH MEMORANDUM

FLIGHT MEASUREMENTS OF HORIZONTAL-TAIL LOADS ON THE DOUGLAS X-3 RESEARCH AIRPLANE

By Harriet J. Stephenson

SUMMARY

Flight measurements of the horizontal-tail loads on the Douglas X-3 research airplane during wind-up turns, pull-ups, and stabilizer pulses were made over an altitude range from 27,000 to 33,000 feet and throughout a Mach number range from 0.65 to 1.16. The results of these measurements are presented in this paper.

The normal-force-curve slope of the horizontal-tail panel $\left(C_{N_\alpha}\right)_t$, derived from stabilizer pulses, had a maximum value of 0.082 and occurred at a Mach number of 0.925. At a Mach number of 1.00 the value of the slope decreased to 0.063 and for higher Mach numbers again increased with Mach number.

Balancing-tail loads, downwash at the tail, and total airplane pitching moments were obtained from pull-ups and wind-up turns. Balancing-tail loads varied nonlinearly with airplane normal-force coefficient throughout the lift range; the wing fuselage was stable for the moderate lift range with increasing stability for increasing Mach number. An increase in stability occurred at lift coefficients between 0.2 and 0.4. The wing-fuselage became unstable at the high lift coefficients.

Downwash varied nonlinearly with angle of attack. An increase in the variation of downwash with angle of attack $d\epsilon/d\alpha$ or a decrease in tail stability occurred at angles of attack between 4° and 8°.

The total airplane pitching moment also displayed nonlinear variations with angle of attack. The airplane became unstable at angles of attack between 7° and 13°.

INTRODUCTION

In recent years the design of the horizontal tail has become increasingly complex because of the nonlinear variation in tail loads with Mach number and airplane lift throughout the transonic speed range.

Existing theoretical methods do not accurately predict these variations, therefore experimental data are required and are being obtained on research airplanes embodying various wing-body combinations.

As part of the cooperative Air Force-Navy-NACA research program on the Douglas X-3 airplane, flight investigations were made at the NACA High-Speed Flight Station at Edwards, Calif. to determine the structural and aerodynamic loads, lift and drag, and dynamic and static stability and control. Preliminary results obtained during the manufacturer's demonstration flights and U. S. Air Force evaluation flights presenting lift and drag and stability and control characteristics are reported in references 1 and 2, respectively. Results of NACA flight tests to determine horizontal-tail loads during longitudinal maneuvers over a Mach number range from 0.65 to 1.16 are presented in this paper.

SYMBOLS

BM	bending moment of right horizontal tail, ft-lb
b_t	horizontal-tail panel semispan, ft
C_b	bending-moment coefficient of right horizontal-tail panel, $BM/q^*S_t b_t$
C_m	total airplane pitching-moment coefficient
C_{m_w}	pitching-moment coefficient of left wing panel, $M_w/q^*S_w\bar{c}$
$C_{m_{wf}}$	wing-fuselage pitching-moment coefficient
C_N	normal-force coefficient of right horizontal-tail panel, L_{t_R}/q^*S_t
C_{N_A}	airplane normal-force coefficient, nW/q^*S
C_{N_t}	horizontal-tail normal-force coefficient, L_t/q^*S_t

$C_{N_{t_{Bal}}}$ tail normal-force coefficient required to balance wing-fuselage pitching-moment coefficient, $L_{t_{Bal}}/q^*S_t$

C_{N_w} normal-force coefficient of left wing panel, L_w/q^*S_w

$\left(C_{N_\alpha}\right)_t$ horizontal-tail panel normal-force-curve slope, per deg

c_{p_A} center of pressure of additional airload, percent horizontal-tail panel semispan

$\bar{c}$ wing mean aerodynamic chord, ft

g acceleration due to gravity, ft/sec^2

h_p pressure altitude, ft

i_t stabilizer setting, deg (positive, leading edge up)

L_t aerodynamic tail load, lb (positive, load up)

L_{t_R} aerodynamic load on right horizontal tail

L_w aerodynamic load on left wing panel

$L_{t_{Bal}}$ aerodynamic tail load required to balance wing-fuselage pitching moment, lb

l_t tail length, ft (measured from airplane center of gravity to quarter-chord station of tail panel mean aerodynamic chord)

M Mach number

M_w pitching moment of left wing panel, ft-lb

n normal acceleration, g units

q pitching angular velocity (positive, nose up), radians/sec

$\dot{q}$ pitching angular acceleration, radians/sec^2

q^* dynamic pressure, $\frac{1}{2}\rho V^2$, lb/sq ft

q^*_t dynamic pressure at the tail, lb/sq ft

S	wing area, sq ft
S_t	horizontal-tail-panel area, sq ft
S_w	wing-panel area, sq ft
t	time, sec
W	airplane gross weight, lb
α	angle of attack, deg
$\dot{\alpha}$	time rate of change of angle of attack, $d\alpha/dt$, deg/sec
ϵ	downwash angle, deg

DESCRIPTION OF AIRPLANE

The X-3 is a single-place research airplane designed for flight at supersonic speeds. It has an all-movable horizontal stabilizer with an aspect ratio of 4.33 and straight wings with aspect ratio 3.09, both employing modified hexagonal airfoil sections of 4.5-percent thickness. The controls are powered by an irreversible boost system with artificial feel.

Figure 1 shows a three-view drawing of the airplane and photographs are presented in figure 2. The physical characteristics of the airplane are presented in table I.

INSTRUMENTATION AND ACCURACY

Standard NACA recording instruments were installed in the X-3 airplane to measure the following quantities pertinent to this investigation:

Airspeed
Altitude
Angle of attack
Normal acceleration
Pitching angular velocity and acceleration
Stabilizer position

Bending moment and shear were measured by strain gages located on the horizontal-tail spar 11 inches outboard of the center line, as shown

in figure 1. Strain-gage outputs were recorded on a 36-channel oscillograph. All instruments were correlated by a common timer.

The accuracy of the shear and bending-moment measurements was estimated to be ±100 pounds and ±1,500 inch-pounds, respectively.

Angle of attack was measured by a vane located on the nose boom. No corrections were made for boom bending or pitching velocity. The maximum error due to pitching velocity encountered in these maneuvers was approximately 0.65°; however, for most of the data the error was much less. Stabilizer angle was estimated to be accurate to $\pm 0.15^{\circ}$ and pitching velocity to approximately ±0.01 radian/sec. For pitching accelerations less than 0.2 radian/sec^2 the accuracy was estimated to be ±0.02 radian/sec^2. For higher acceleration the maximum error was approximately 10 percent of the measured value. The errors in $C_{N_{t_{Bal}}}$ caused by the error in pitching angular acceleration are within the accuracy of $C_{N_{t_{Bal}}}$.

The estimated accuracy of other pertinent quantities is:

Mach number	±0.01
Normal acceleration	±0.05g
C_{N_A}	±0.02

PROCEDURE

Aerodynamic loads were obtained by correcting the measured tail loads for the inertia of the tail. Balancing-tail-load coefficients were obtained from wind-up turns and pull-ups by correcting the aerodynamic tail-load coefficients to zero pitching acceleration.

The normal-force-curve slope of the horizontal-tail panel $\left(C_{N_\alpha}\right)_t$ was determined from the initial portion of abrupt stabilizer pulses. The X-3 airplane employs an all-movable stabilizer, therefore $\left(C_{N_\alpha}\right)_t$ was obtained by dividing the maximum increment of tail-load coefficient by the corresponding increment of stabilizer angle. Angle of attack had not changed appreciably up to the maximum load, and the maximum error caused by the change in pitching velocity was estimated to be approximately 20 percent.

The downwash angle was derived from the equation

$$C_{N_t} = \left(C_{N_\alpha}\right)_t \left[\alpha - \epsilon + i_t + q\frac{l_t}{V} + \dot{\alpha}\frac{l_t}{V}\frac{d\epsilon}{d\alpha}\right]$$

where C_{N_t}, α, i_t, q, and V were measured during pull-ups and wind-up turns. For these calculations the effect of $\dot{\alpha}$ was considered to be small, therefore the equation used to calculate downwash was

$$\epsilon = \alpha + i_t + q\frac{l_t}{V} - \frac{C_{N_t}}{\left(C_{N_\alpha}\right)_t}$$

The contribution of the horizontal tail to the airplane stability is given by $\left(C_{N_\alpha}\right)_t(\alpha - \epsilon)$. The wing-fuselage pitching-moment characteristics, determined from balancing-tail loads, were combined with $\left(C_{N_\alpha}\right)_t(\alpha - \epsilon)$ to give the total airplane pitching-moment variation with angle of attack. Assuming q^*_t/q^* to be 1.0, the total airplane pitching moment is given by the equation

$$C_m = \left[-\left(C_{N_\alpha}\right)_t(\alpha - \epsilon) + C_{N_{t_{Bal}}}\right]\frac{l_t S_t}{S\bar{c}}$$

TESTS

Horizontal-tail loads were measured on the X-3 airplane during pull-ups, wind-up turns, and stabilizer pulses over a Mach number range from 0.65 to 1.16 and an altitude range from 27,000 to 33,000 feet. A few stabilizer pulses were made at altitudes of 18,000 and 20,000 feet.

The center-of-gravity position was estimated to be between 3 and -2 percent mean aerodynamic chord. Reynolds number based on the mean aerodynamic chord of the horizontal tail varied from about 5.5×10^6 to about 12.5×10^6 for these tests.

RESULTS AND DISCUSSION

Time histories of angle of attack, pitching velocity and acceleration, tail normal-force coefficients, and stabilizer position for four typical stabilizer pulses are shown in figure 3. From these maneuvers it was possible to derive $(C_{N_\alpha})_t$ by using increments of C_{N_t} and i_t. These increments were taken from the beginning of the pulse to the maximum load.

The horizontal-tail-panel characteristics shown by the variation of $(C_{N_\alpha})_t$ with Mach number are given in figure 4. At a Mach number of 0.65 the value of $(C_{N_\alpha})_t$ is 0.055 and increases to its maximum value of 0.082 at a Mach number of 0.925. At a Mach number of 1.00 $(C_{N_\alpha})_t$ decreases to 0.063. For Mach numbers above 1.00 $(C_{N_\alpha})_t$ again increases. All the stabilizer pulses were made at angles of attack of less than 7°; therefore, the validity of the curve for higher angles of attack is questionable.

Time histories of four typical pull-ups and wind-up turns are presented in figure 5. The variation with angle of attack of the measured data during these pull-ups and wind-up turns is presented in figure 6. These data were used to derive the centers of pressure, balancing-tail loads, downwash angles, and total airplane pitching-moment coefficients.

Shown in figure 7 is bending-moment coefficient plotted against normal-force coefficient for the right horizontal tail. The spanwise center of pressure of the additional load was obtained from the slopes of these curves and is presented as a function of Mach number in figure 8. Slopes were not taken for Mach numbers less than 0.89 because of the limited lift range covered. The spanwise center of pressure moved inboard from approximately 50 percent to 43 percent tail semispan as the Mach number increased from 0.89 to 1.16.

Balancing-tail loads are shown plotted against C_{N_A} in figure 9. For the lower lift region the slope $\frac{dC_{N_{t_{Bal}}}}{dC_{N_A}}$ varies from approximately zero for the lower Mach numbers to approximately -0.24 for a Mach number of 1.10. At the lower Mach numbers there is a sharp increase in $\frac{dC_{N_{t_{Bal}}}}{dC_{N_A}}$ at $C_{N_A} = 0.4$, and as the Mach number increases above 0.89, this change

in slope becomes less pronounced and the C_{N_A} value at which it occurs decreases to about 0.2. At the higher lifts the slopes become positive.

The variation of downwash with angle of attack $d\epsilon/d\alpha$ is given in figure 10. The downwash characteristics indicate a decrease in horizontal-tail stability, or an increase in $d\epsilon/d\alpha$, at an angle of attack of approximately 8° for low Mach numbers and approximately 4° for Mach numbers greater than 0.89. For the higher angles of attack $d\epsilon/d\alpha$ becomes erratic.

The total airplane pitching-moment coefficient plotted against angle of attack is given in figure 11. The airplane pitching-moment curves show stable variations for the lower lift range, becoming unstable at angles of attack between 7° and 13°. For angles of attack above 7° the data are somewhat questionable because the horizontal-tail panel normal-force-curve slopes were measured at lower angles of attack.

Wing-fuselage and airplane pitching moments derived from tail loads are shown in figure 12, together with the wing-panel pitching moment and lift characteristics obtained from unpublished strain-gage data. For the lower Mach numbers there is a sharp increase in the wing-fuselage stability at angles of attack of approximately 8°. For Mach numbers above 0.89 there is a smaller increase in stability at angles of attack near 4°. In general, the trends of C_{m_w}, $C_{m_{wf}}$, and C_m over the angle-of-attack range are similar, with these curves exhibiting increases or decreases in stability at approximately the same values of α. The variation of C_{N_w} with α exhibits a decrease at about the same angle of attack at which the decrease in stability occurs.

Balancing-tail loads plotted against Mach number for various normal-force coefficients are presented in figure 13. For Mach numbers ranging from 0.85 to 1.00 a sharp increase in magnitude of $C_{N_{t_{Bal}}}$ occurs at all values of C_{N_A}. This increase in tail load becomes greater for the higher C_{N_A} values, indicating an abrupt increase in wing-fuselage stability over this Mach number range.

CONCLUSIONS

Flight measurements of the horizontal-tail loads of the X-3 airplane show:

1. The balancing-tail-load coefficients vary nonlinearly with airplane normal-force coefficient throughout the lift range. The wing

fuselage is stable in the moderate lift region with increasing stability for increasing Mach number. An increase in stability occurs at lift coefficients between 0.2 and 0.4, and at the high lift coefficients the wing fuselage becomes unstable.

2. The horizontal-tail panel normal-force-curve slope $(C_{N_\alpha})_t$ increases with Mach number to its maximum value of 0.082 at a Mach number of 0.925, then decreases to a value of 0.063 at a Mach number of 1.00, and for higher Mach numbers again increases with Mach number.

3. The downwash angle is nonlinear with angle of attack over the lift range and indicates a decrease in horizontal-tail stability at angles of attack between 4° and 8°. This decrease corresponds to the lift coefficients at which an increase in wing-fuselage stability occurs.

4. The total airplane pitching moment varies nonlinearly with angle of attack throughout the lift range and indicates positive airplane stability for the lower lift range. The airplane tends to become unstable at angles of attack between 7° and 13°.

High-Speed Flight Station,
National Advisory Committee for Aeronautics,
Edwards, Calif., January 6, 1956.

REFERENCES

1. Bellman, Donald R., and Murphy, Edward D.: Lift and Drag Characteristics of the Douglas X-3 Research Airplane Obtained During Demonstration Flights to a Mach Number of 1.20. NACA RM H54I17, 1954.

2. Day, Richard E., and Fischel, Jack: Stability and Control Characteristics Obtained During Demonstration of the Douglas X-3 Research Airplane. NACA RM H55E16, 1955.

TABLE I.- PHYSICAL CHARACTERISTICS OF THE DOUGLAS X-3 RESEARCH AIRPLANE

Wing:	
Total area, sq ft	166.50
Span, ft	22.69
Mean aerodynamic chord, ft	7.84
Aspect ratio	3.09
Taper ratio	0.39
Incidence, deg	0
Dihedral, deg	0
Sweep at 0.75 chord line, deg	0
Airfoil section	Modified hexagon
Airfoil thickness ratio, percent chord	4.5
Airfoil leading- and trailing-edge angles, deg	8.58
Horizontal tail:	
Area, sq ft	43.24
Span, ft	13.77
Mean aerodynamic chord, ft	3.34
Aspect ratio	4.38
Taper ratio	0.405
Dihedral, deg	0
Sweep at trailing edge, deg	0
Airfoil section	Modified hexagon
Airfoil thickness ratio outboard of station 26, percent chord	4.50
Airfoil thickness at root chord, percent chord	8.01
Stabilizer travel, leading edge up, deg	6
Stabilizer travel, leading edge down, deg	17
Horizontal-tail panel:	
Area, sq ft	35.36
Semispan, ft	5.47
Mean aerodynamic chord, ft	3.12
Fuselage station of leading edge of mean aerodynamic chord	687.32
Tail length	22.48
Vertical tail:	
Area, sq ft	23.73
Span, ft	5.59
Mean aerodynamic chord, ft	4.69
Aspect ratio	1.32
Taper ratio	0.29
Sweep at leading edge, deg	45
Airfoil section	Modified hexagon
Airfoil thickness ratio, percent chord	4.5
Airfoil leading- and trailing-edge angles, deg	8.58
Fuselage:	
Length, ft	66.75
Maximum width, ft	6.08
Maximum height, ft	4.81
Power plant:	
Engines	Two J34-WE-17 with afterburner
Rating, each engine:	
Static sea-level military thrust, lb	3,370
Static sea-level maximum thrust, lb	4,850
Weight:	
Basic (without fuel, oil, water, pilot), lb	16,120
Total, lb	22,100
Moment of inertia about Y-axis, slug-ft^2	70,000

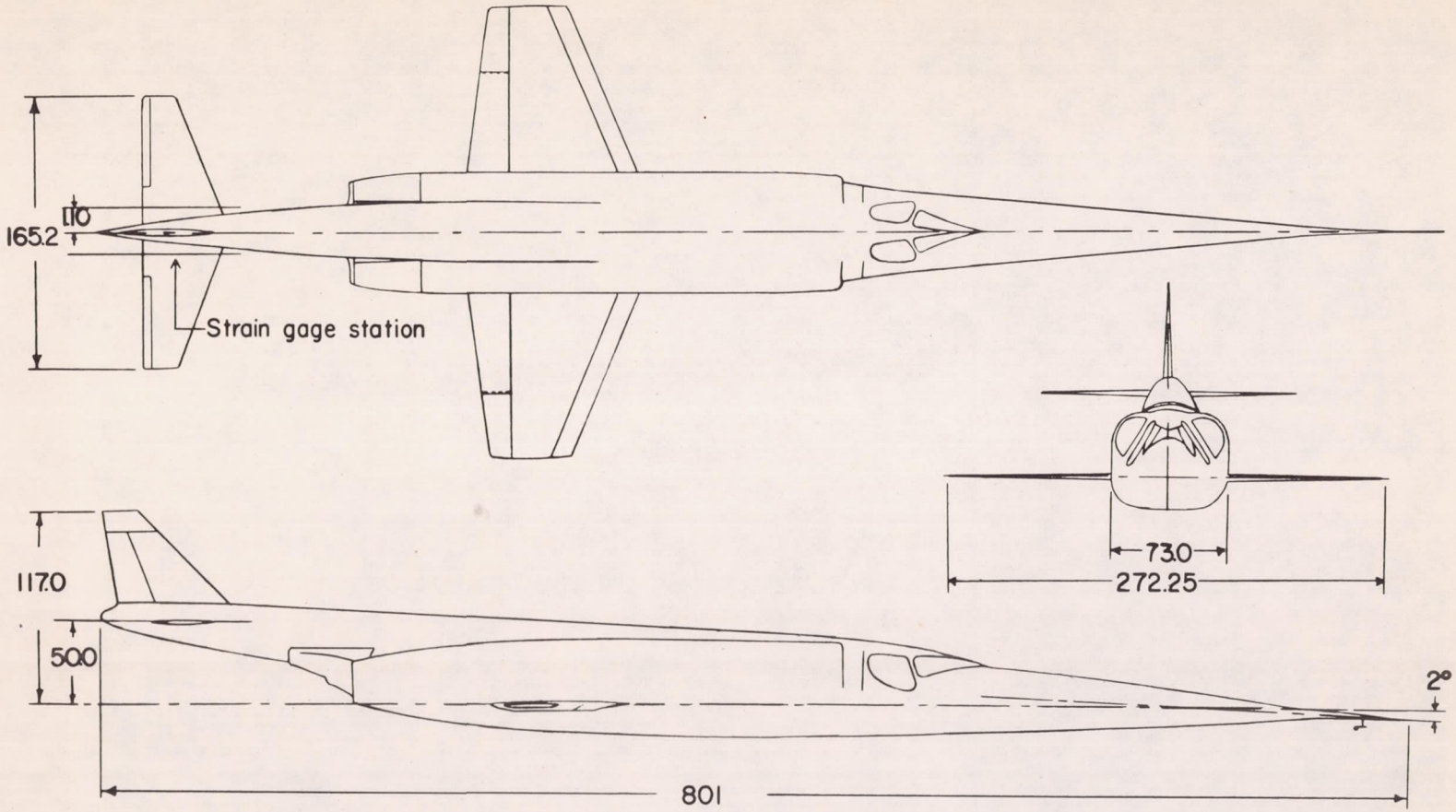

Figure 1.- Three-view drawing of the X-3 airplane. All dimensions in inches.

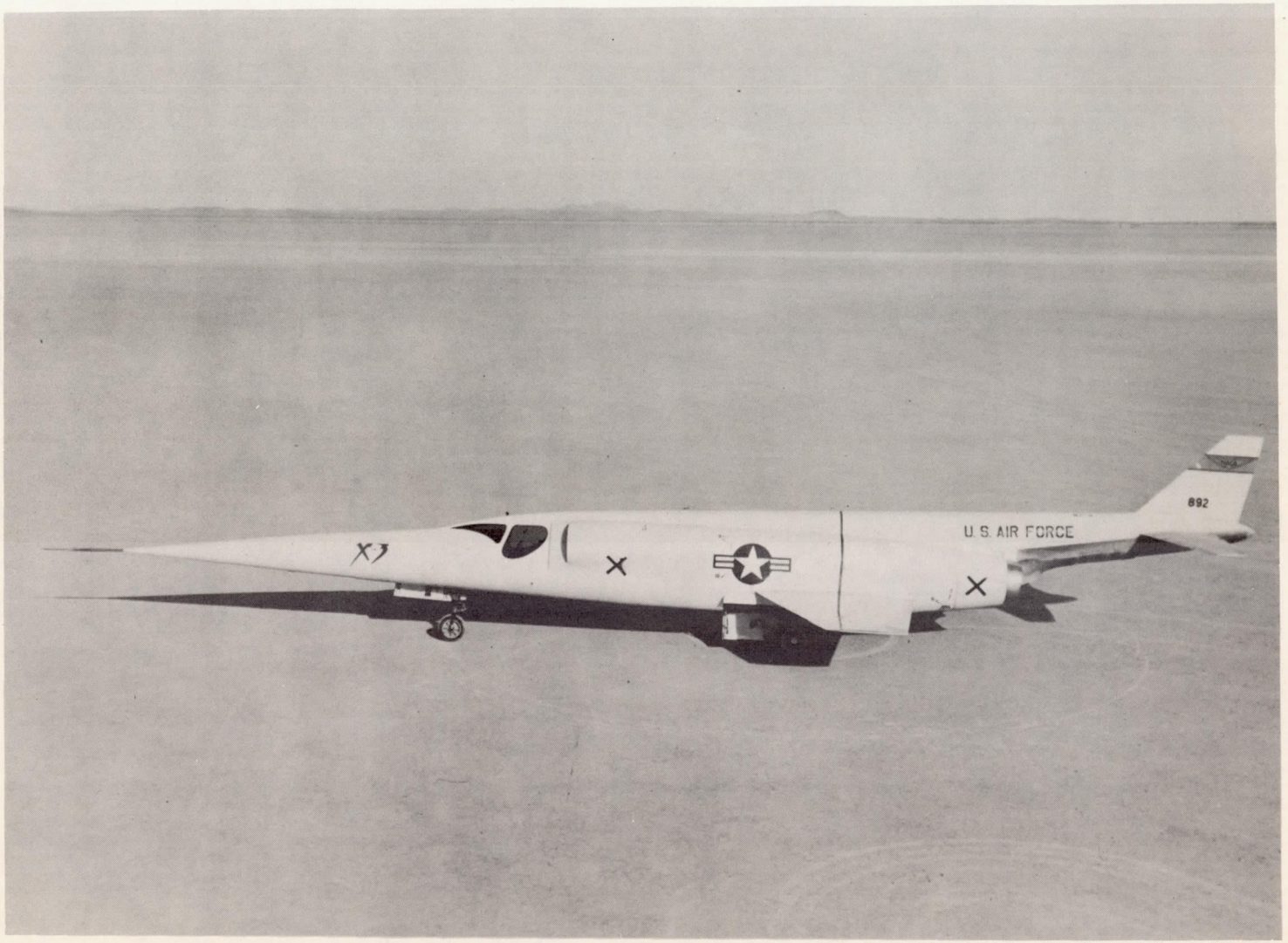

Figure 2.- Side-view photograph of the Douglas X-3 research airplane. L-91756

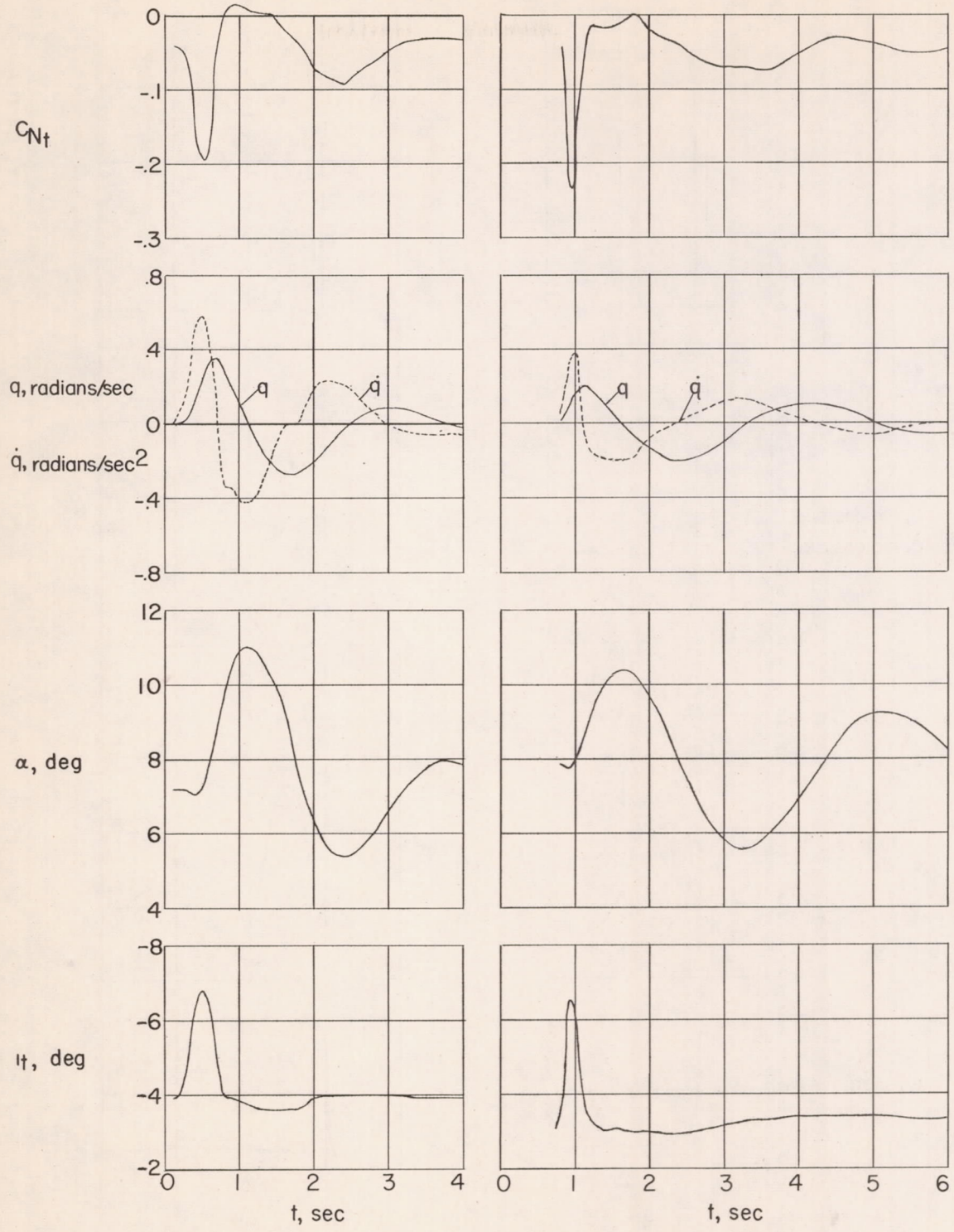

(a) M = 0.66; h_p = 18,000 feet. (b) M = 0.75; h_p = 32,000 feet.

Figure 3.- Typical time histories of stabilizer pulses.

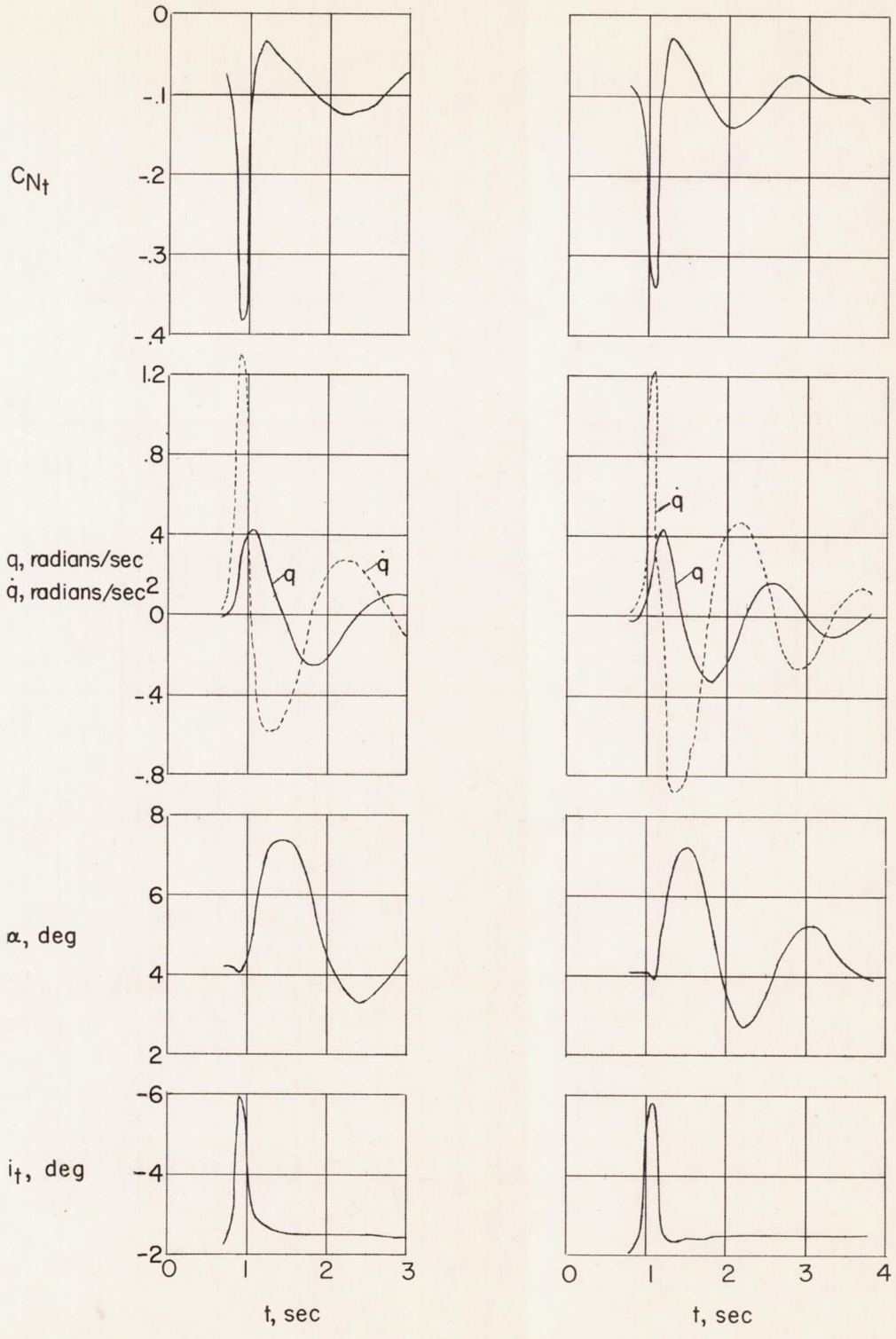

(c) M = 0.92; h_p = 30,000 feet. (d) M = 1.11; h_p = 26,000 feet.

Figure 3.- Concluded.

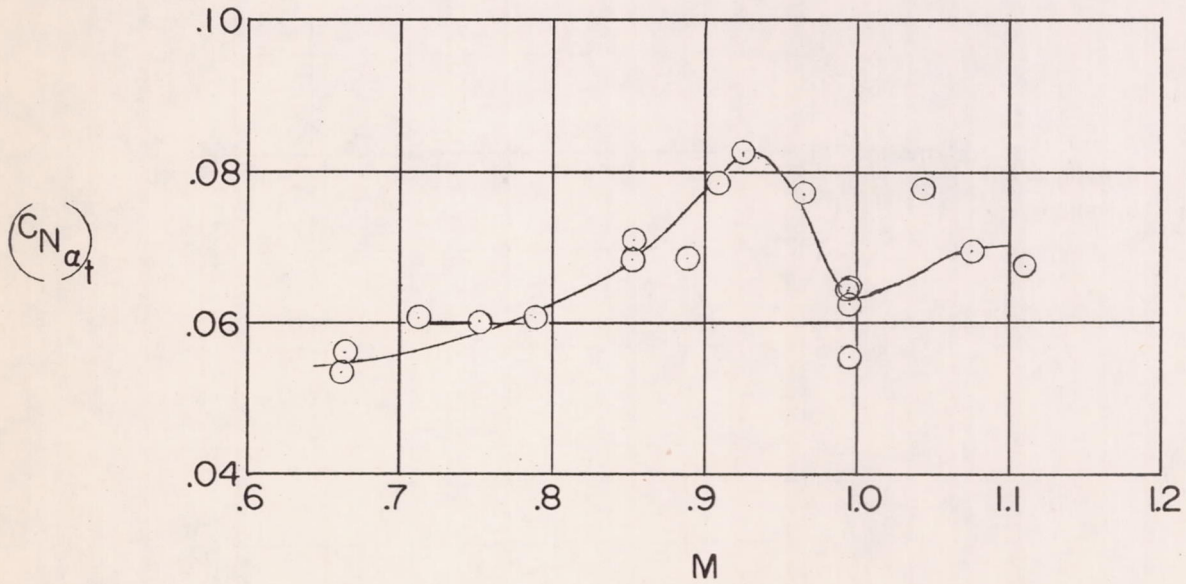

Figure 4.- Variation of normal-force-curve slope of horizontal-tail panel with Mach number.

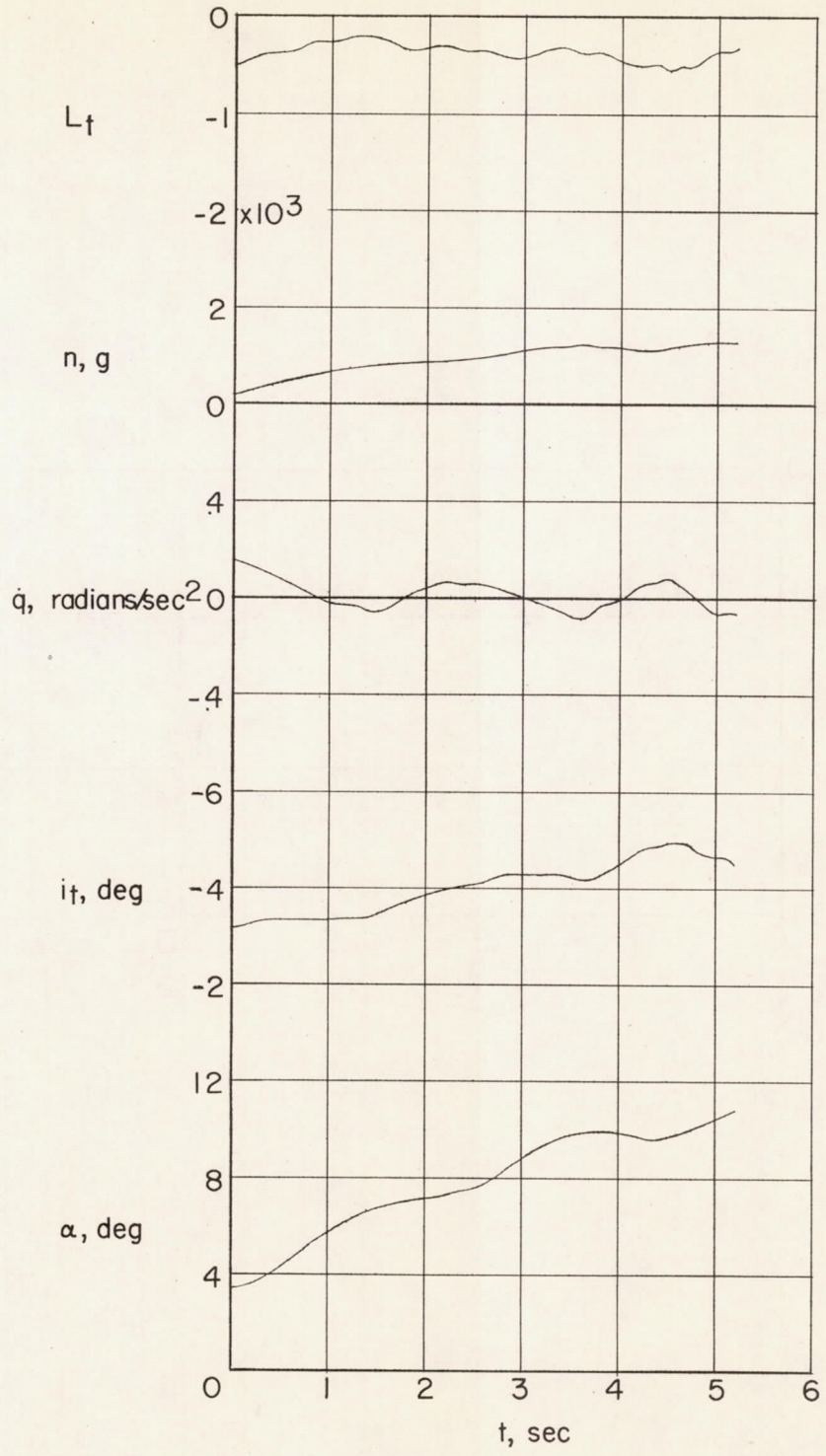

(a) $M \approx 0.77$.

Figure 5.- Time histories of wind-up turns and pull ups at representative Mach numbers.

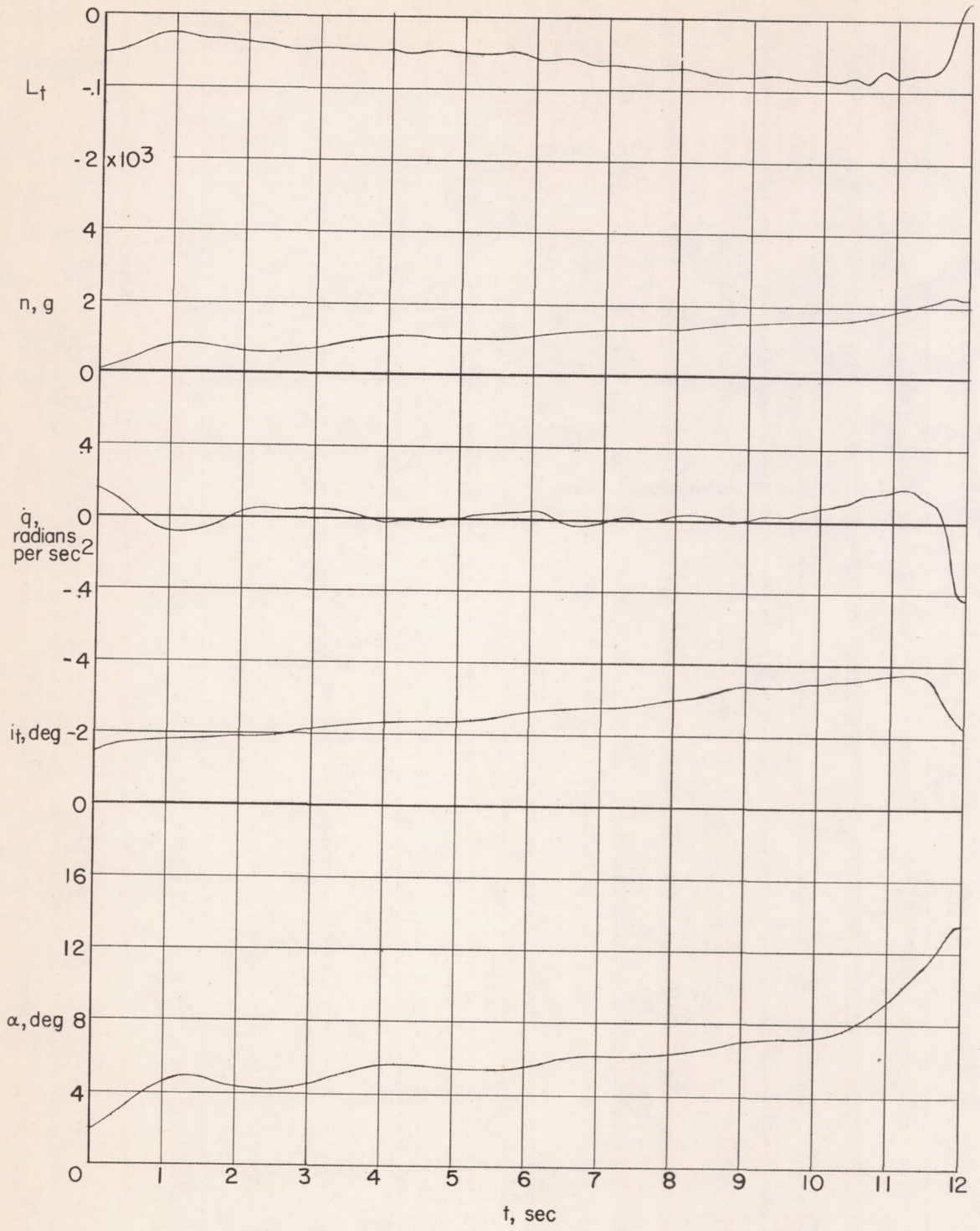

(b) $M \approx 0.89$.

Figure 5.- Continued.

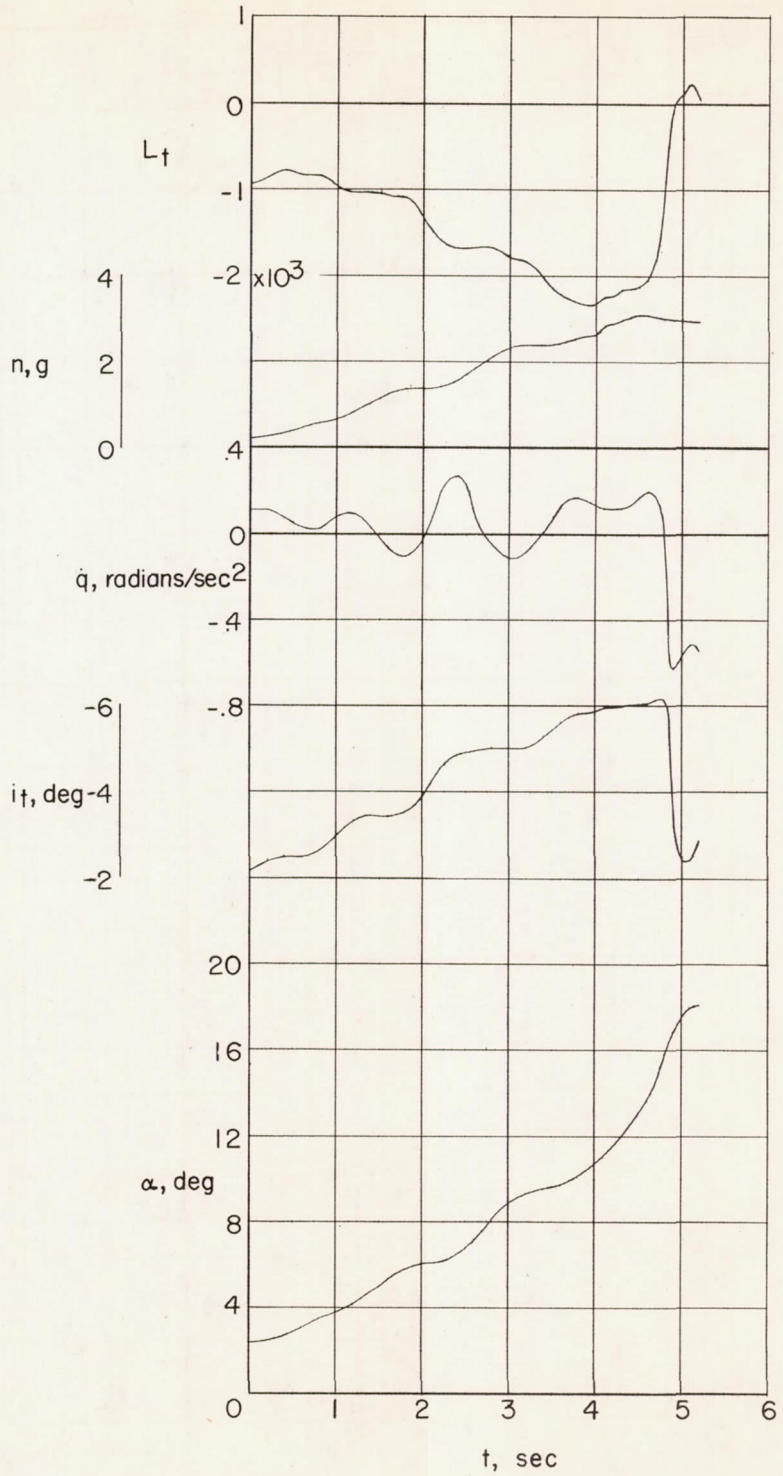

(c) $M \approx 0.95$.

Figure 5.- Continued.

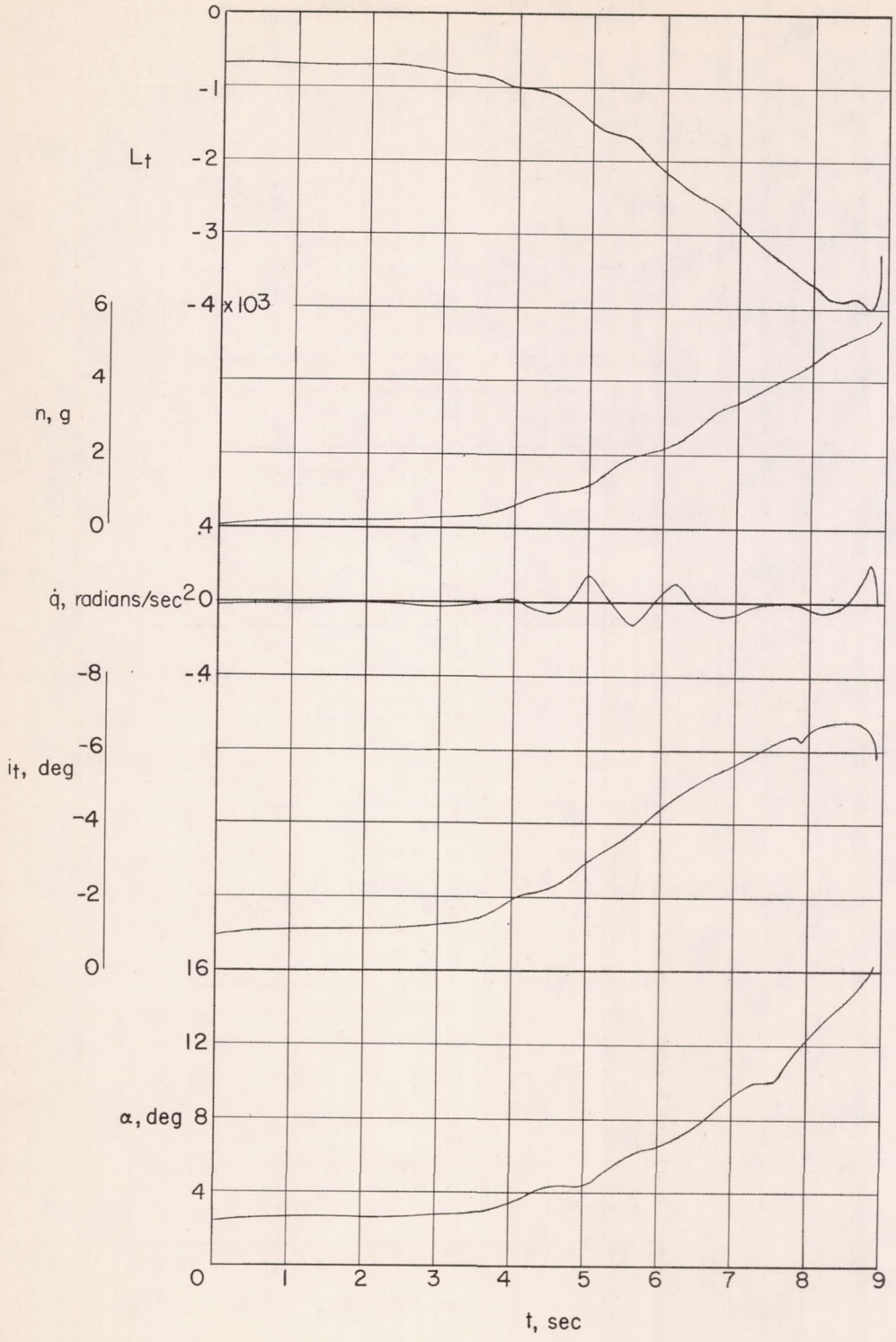

(d) $M \approx 1.10$.

Figure 5.- Concluded.

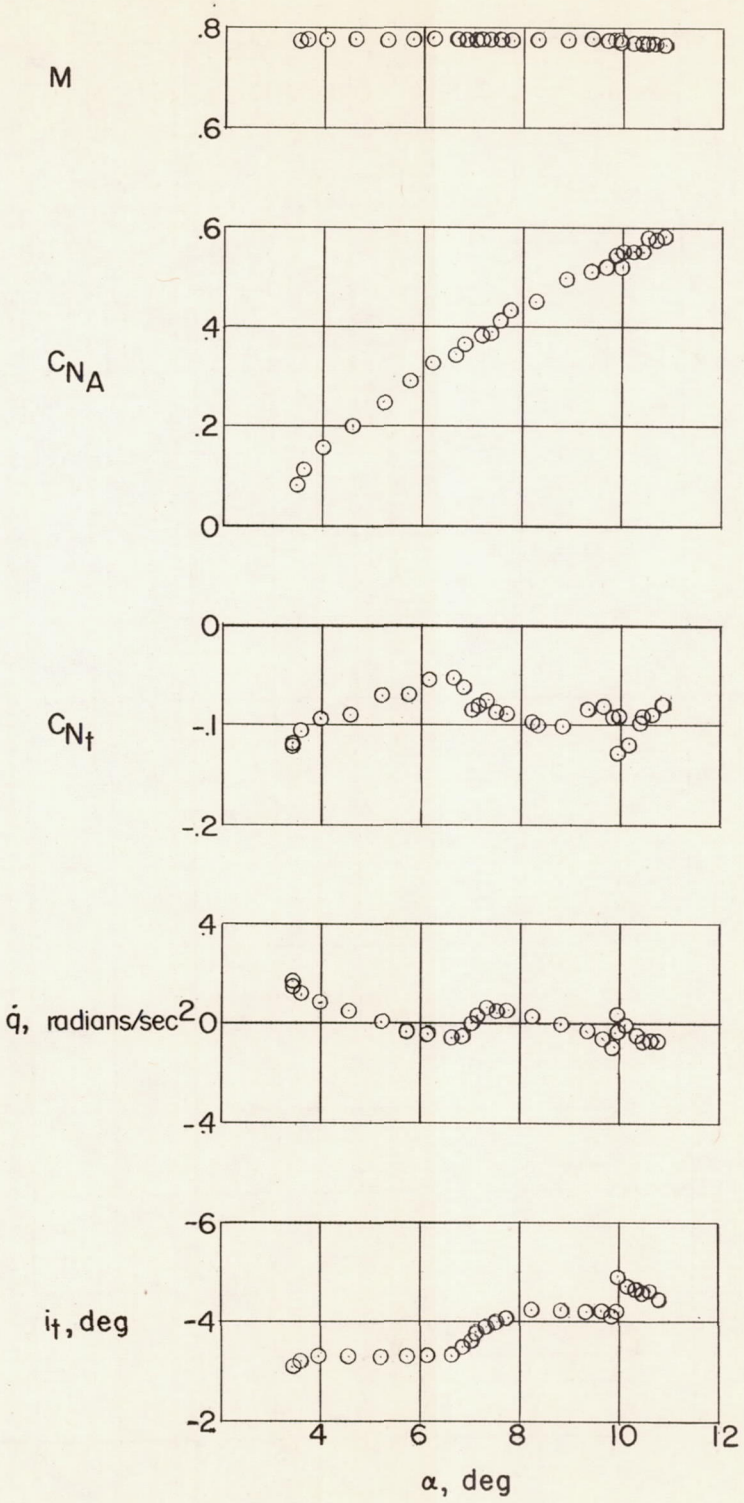

(a) M = 0.77.

Figure 6.- Variation of measured quantities with indicated angle of attack.

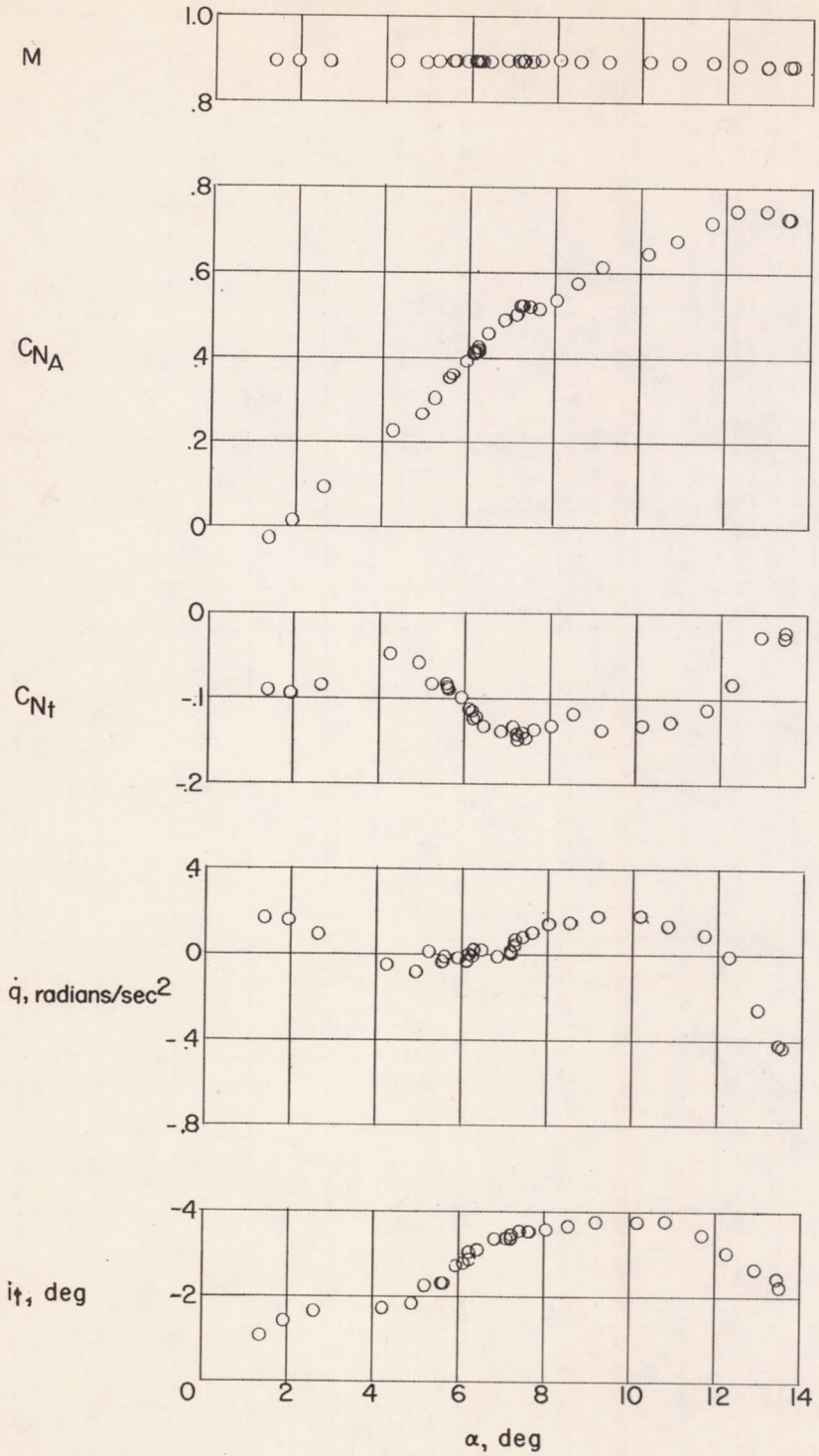

(b) M = 0.89.

Figure 6.- Continued.

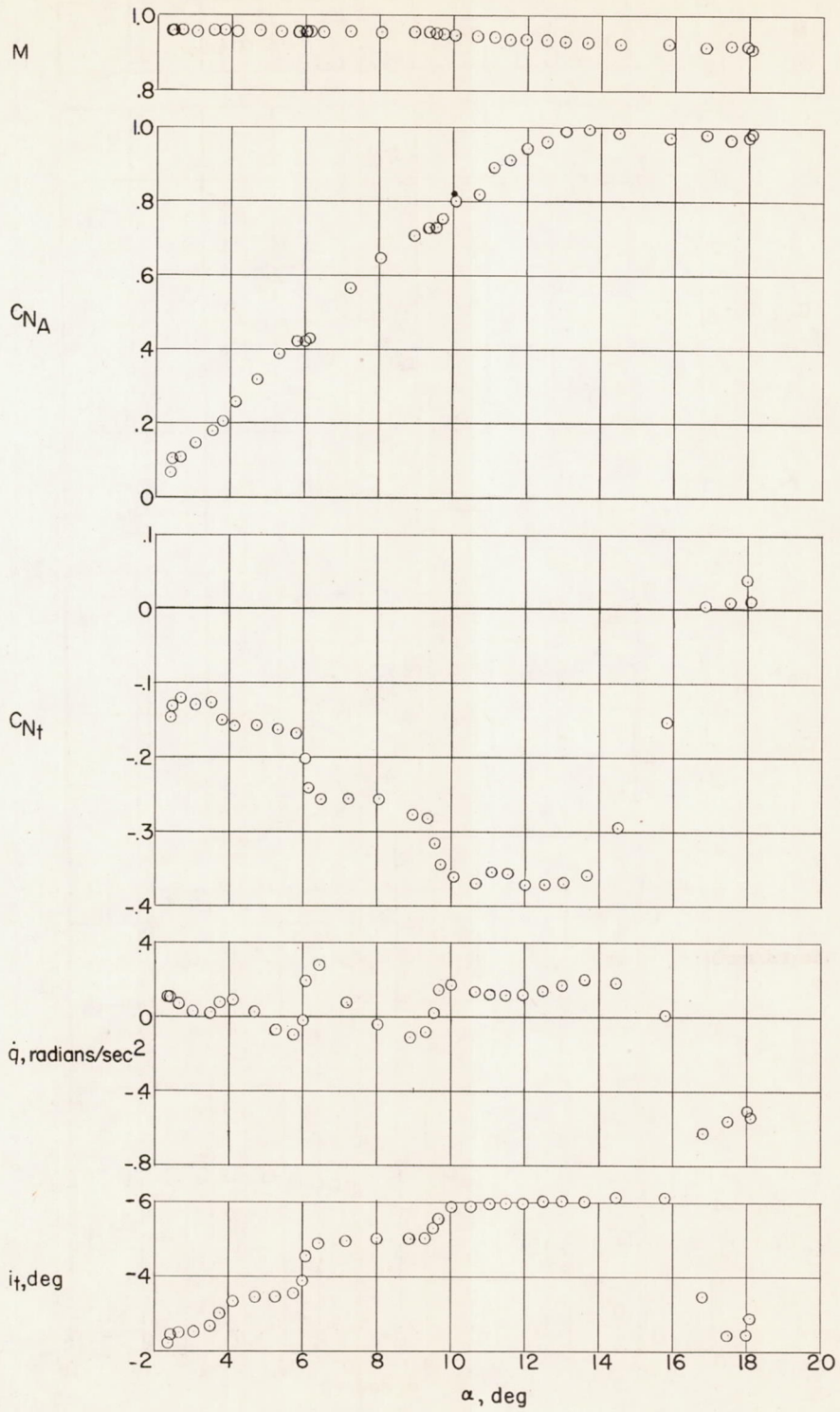

(c) $M \approx 0.95$.

Figure 6.- Continued.

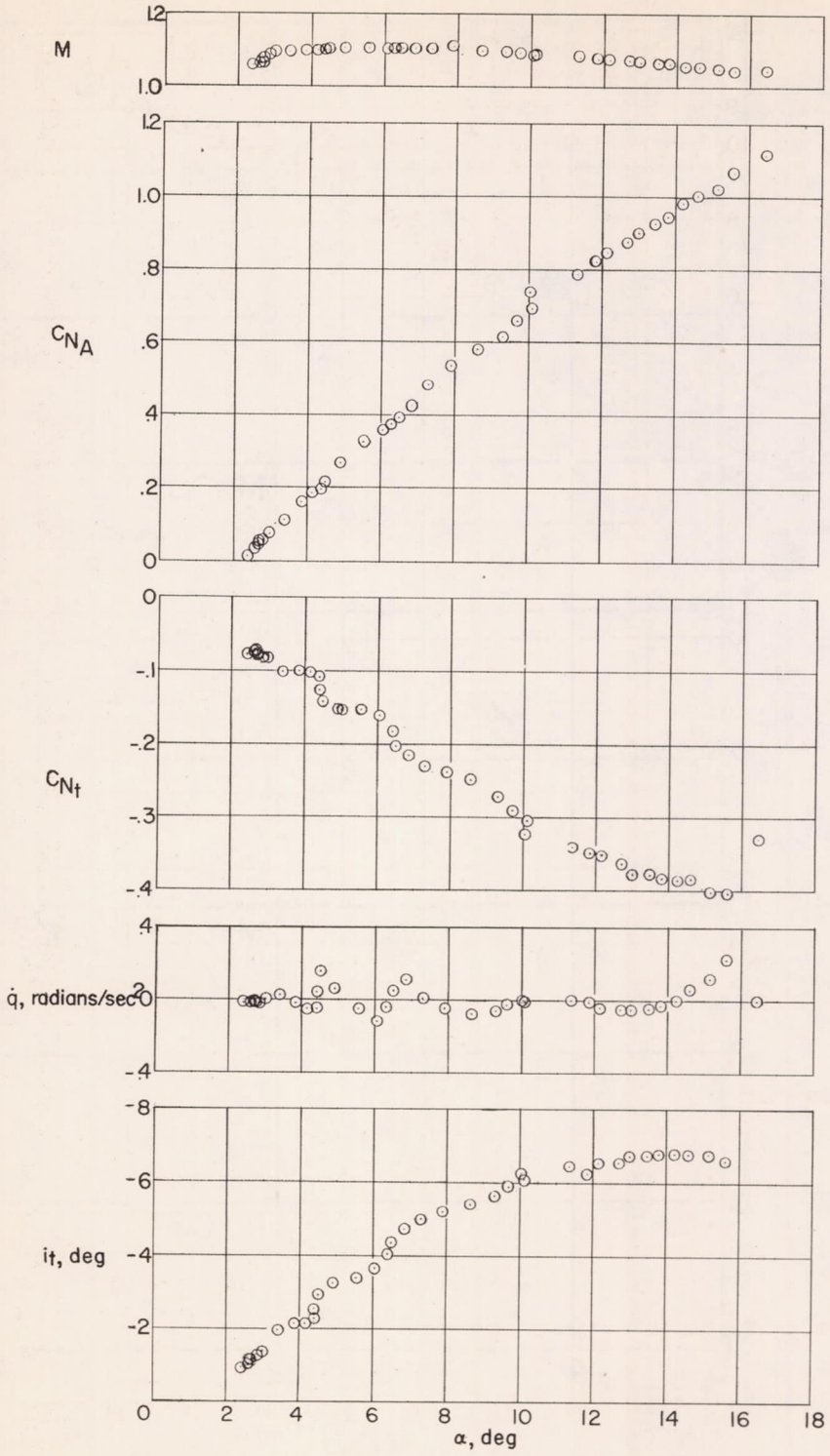

(d) M = 1.10.

Figure 6.- Concluded.

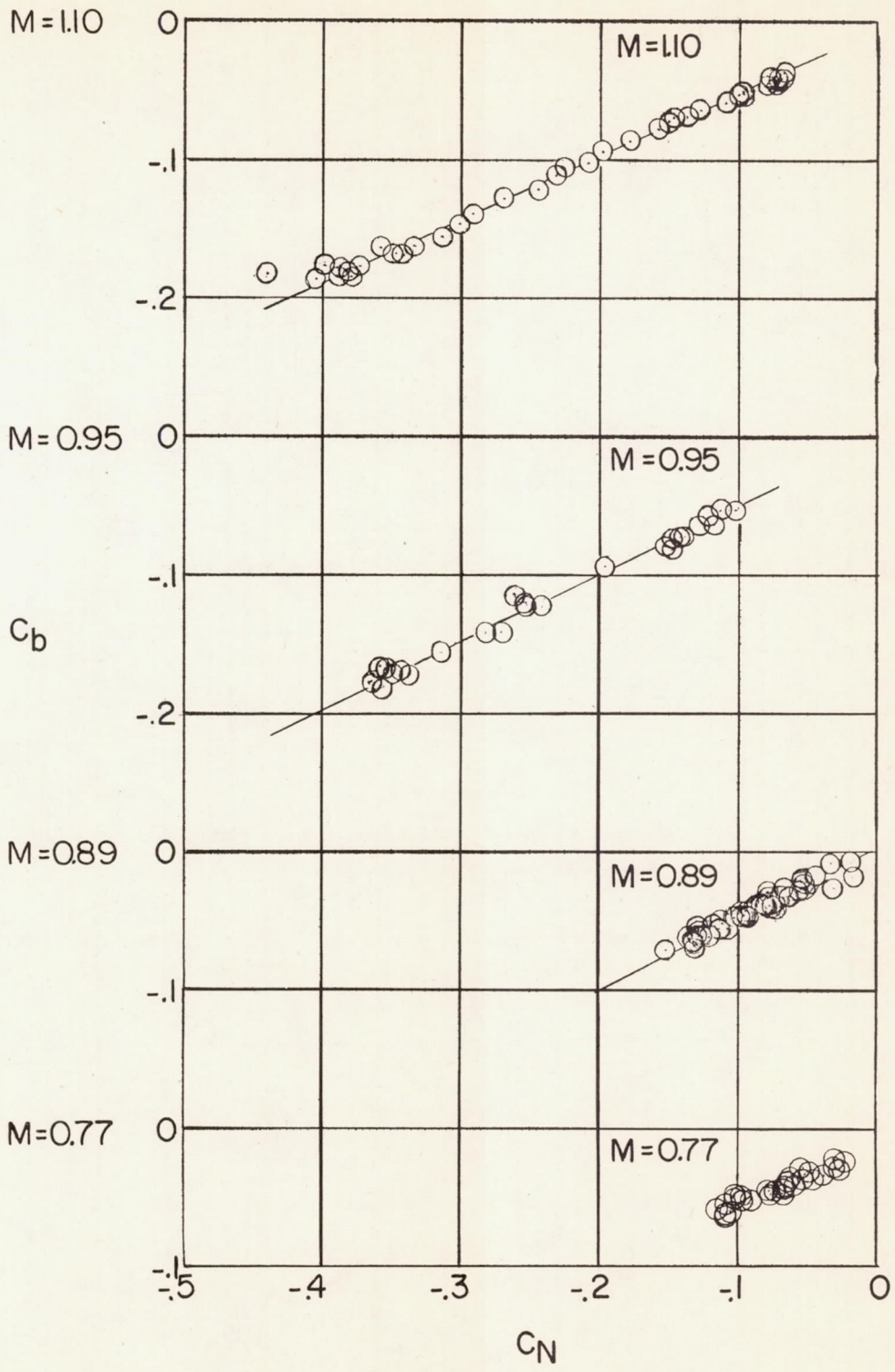

Figure 7.- Variation of bending-moment coefficient with normal-force coefficient. Right horizontal-tail panel.

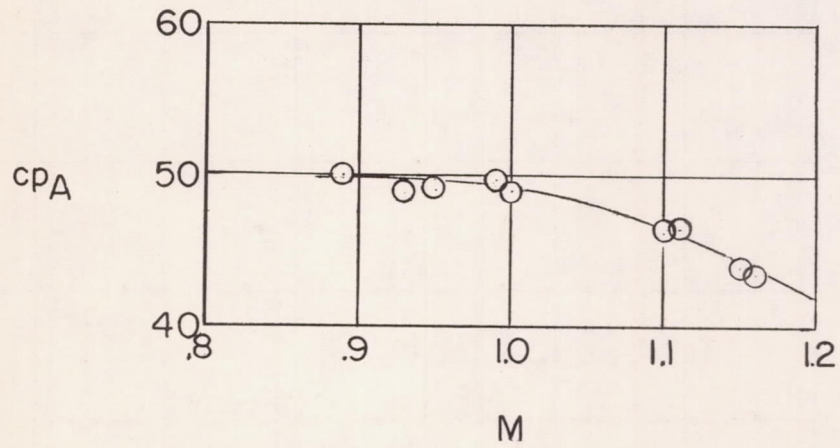

Figure 8.- Variation of spanwise center of pressure of the horizontal-tail panel additional air load with Mach number.

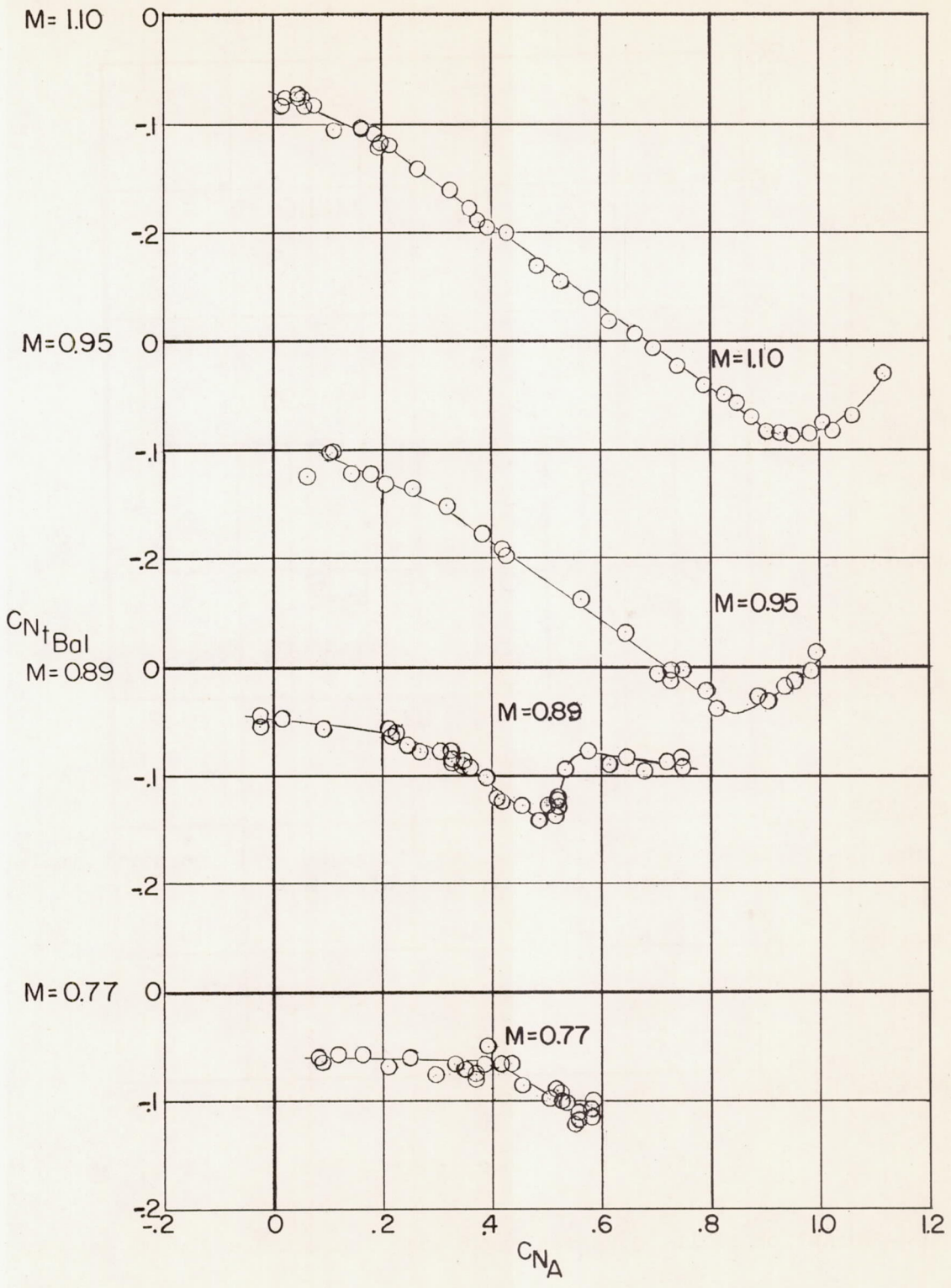

Figure 9.- Variation of the balancing-tail-load coefficients with the normal-force coefficients of the airplane.

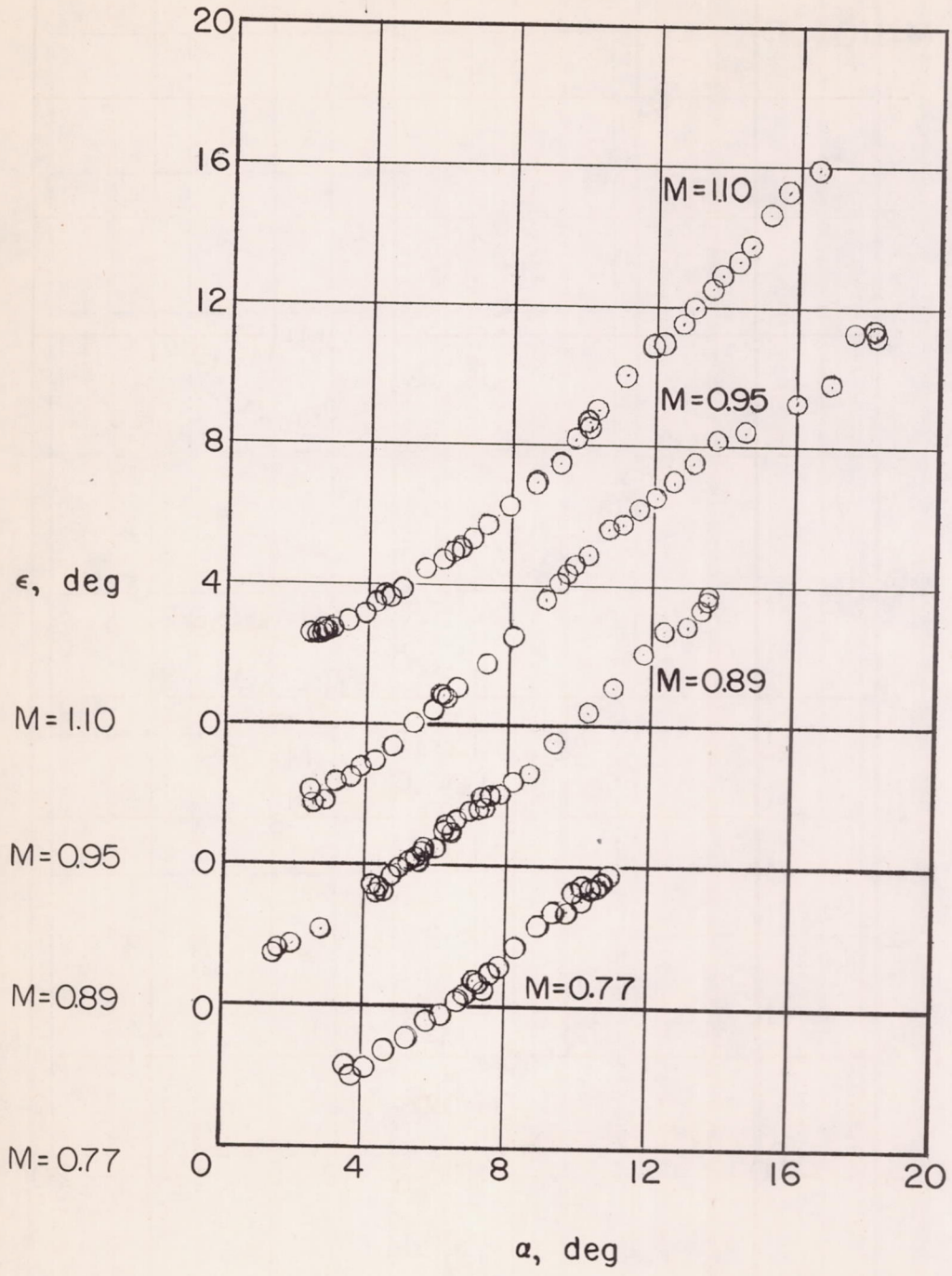

Figure 10.- Variation of the downwash angle with indicated angle of attack.

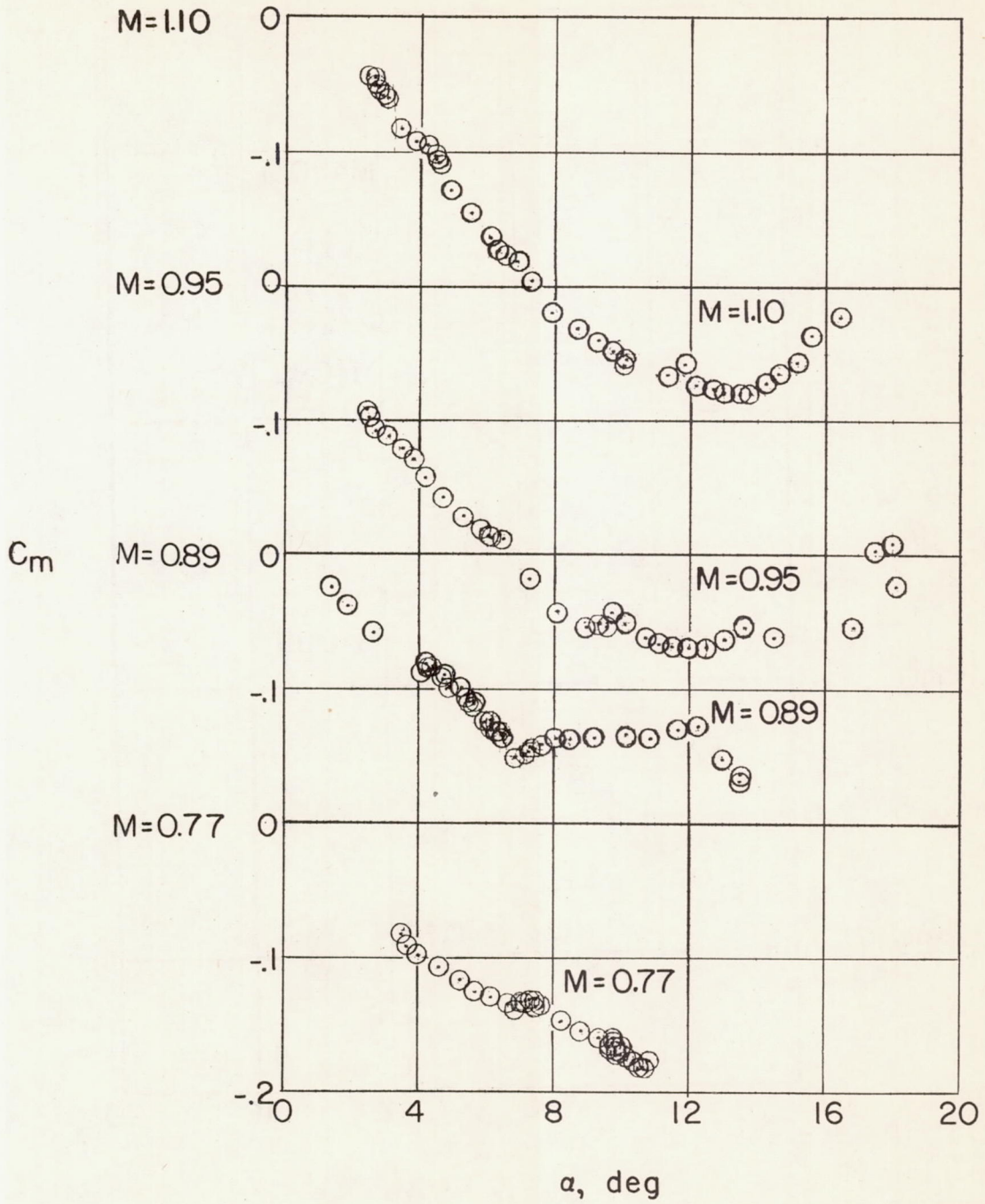

Figure 11.- Variation of total airplane pitching-moment coefficients with indicated angle of attack.

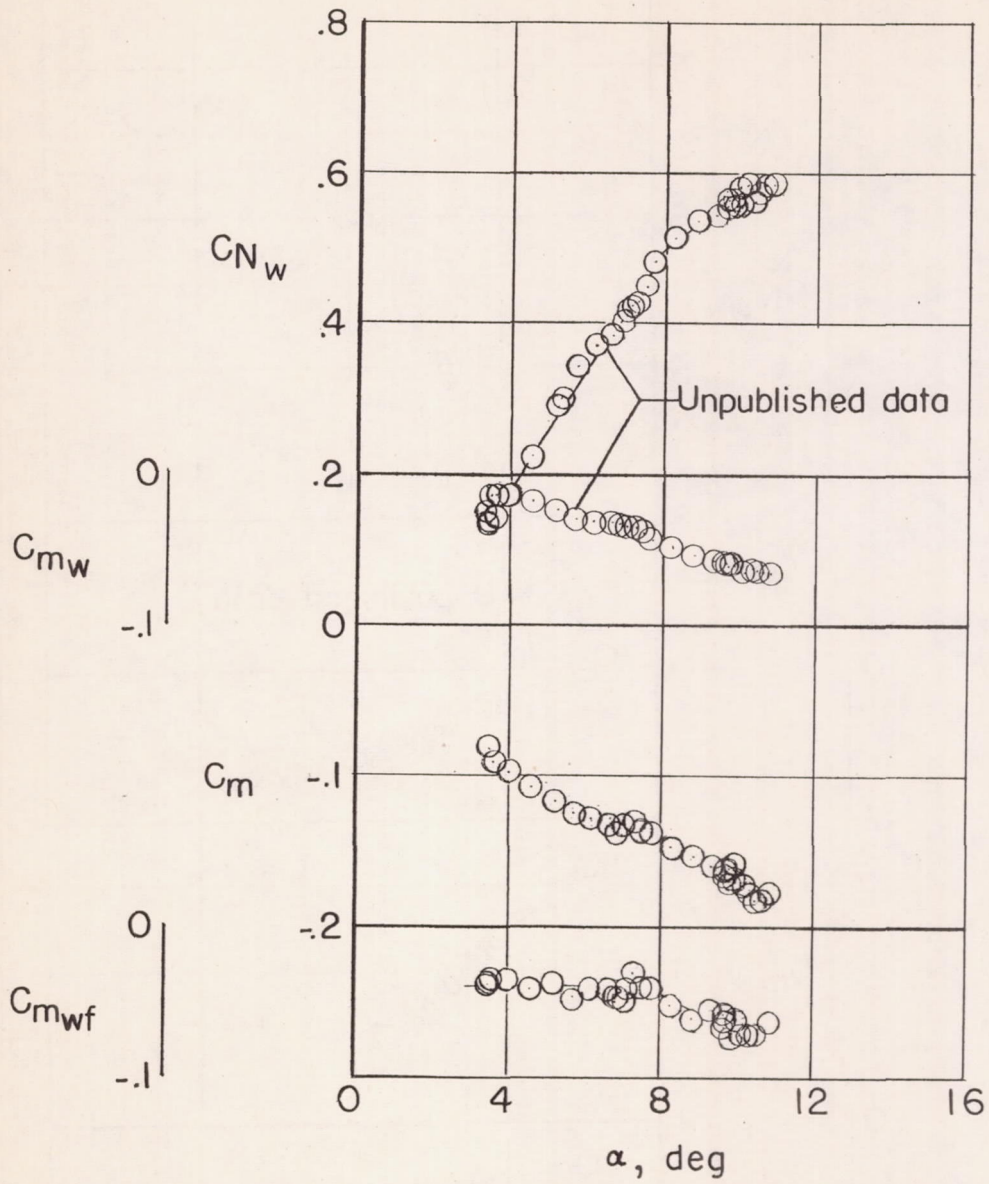

(a) M ≈ 0.77.

Figure 12.- Variation with angle of attack of wing normal-force coefficient and wing, wing fuselage and total airplane pitching-moment coefficient.

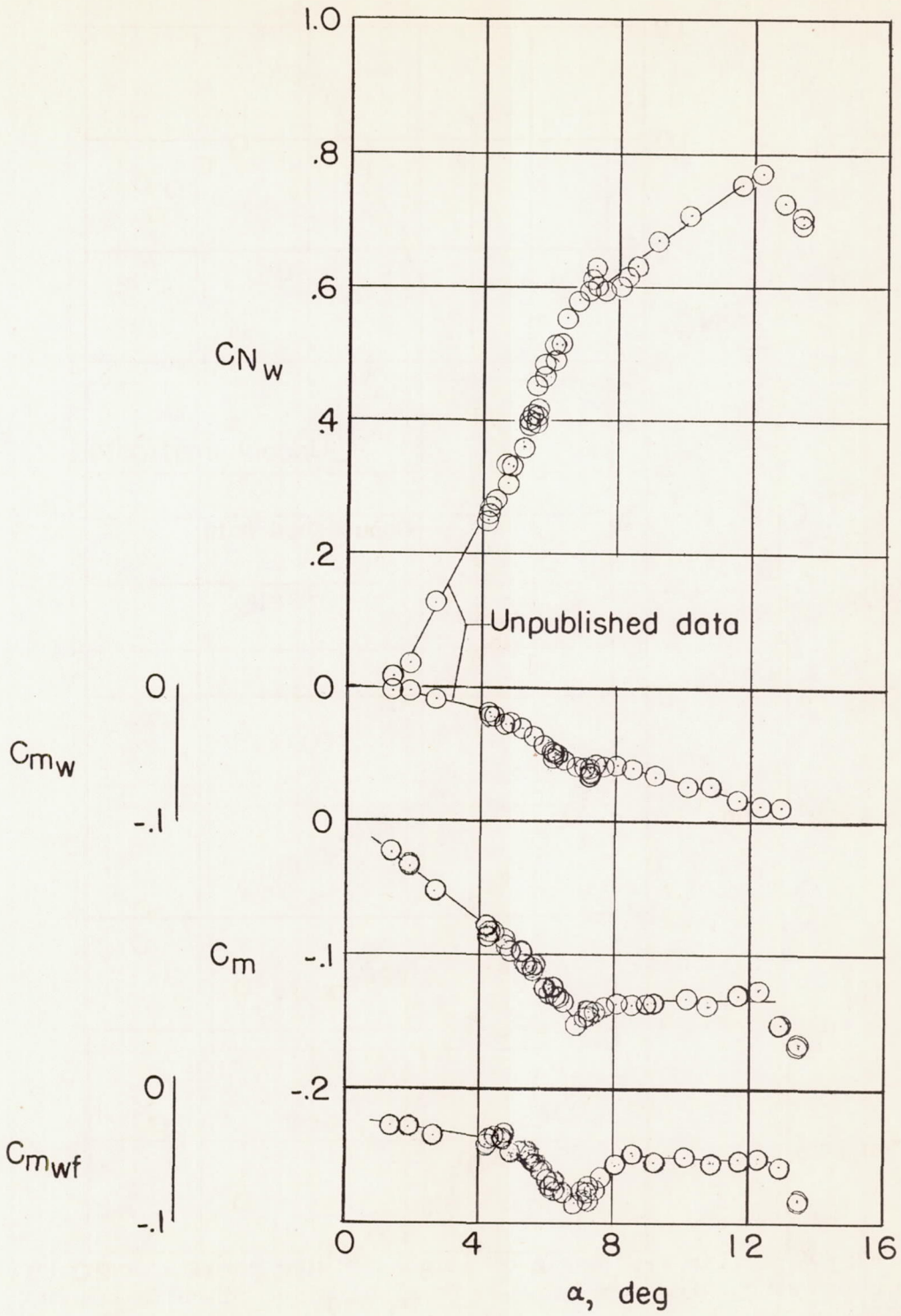

(b) $M \approx 0.89$.

Figure 12.- Continued.

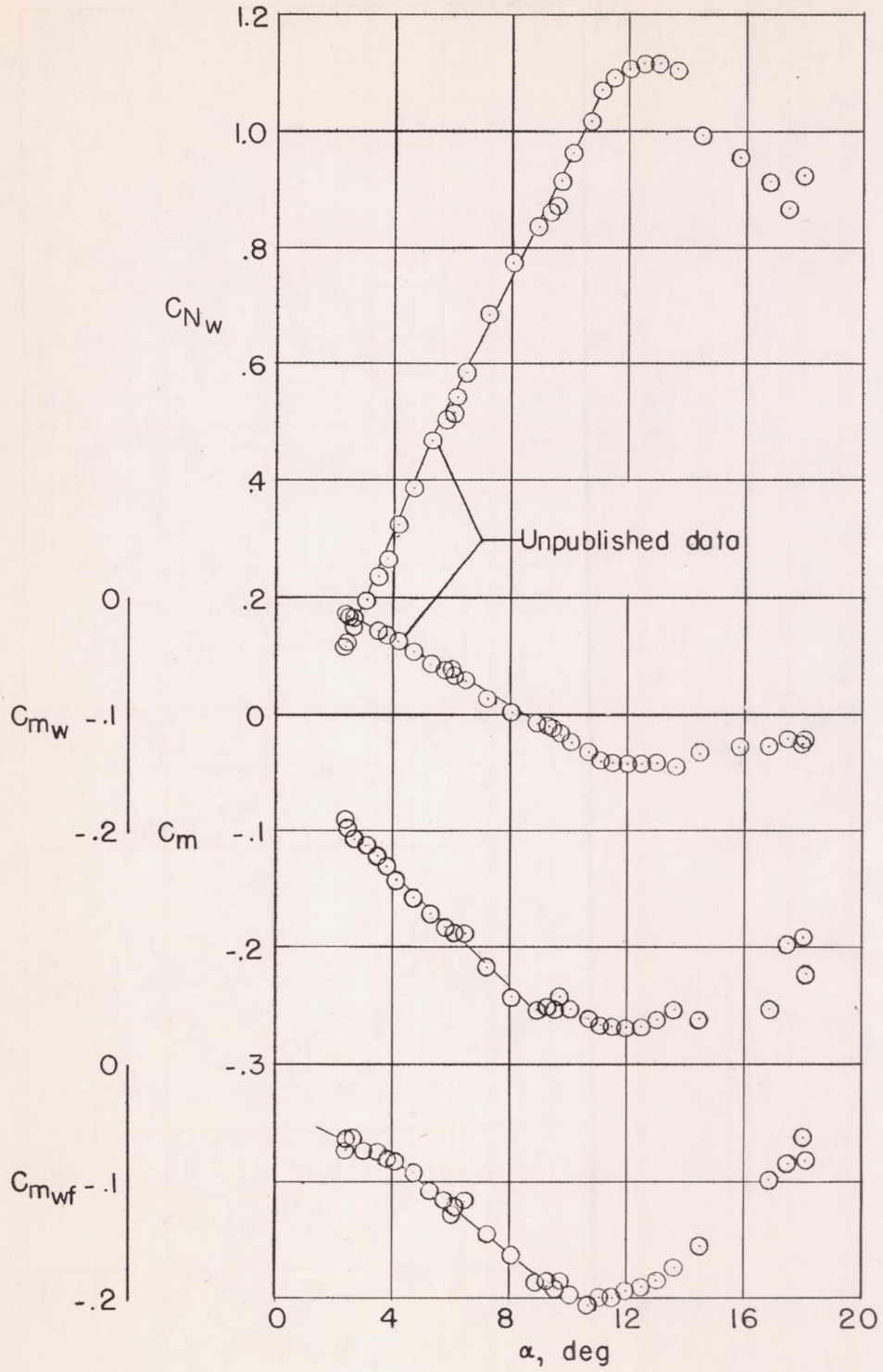

(c) $M \approx 0.95$.

Figure 12.- Continued.

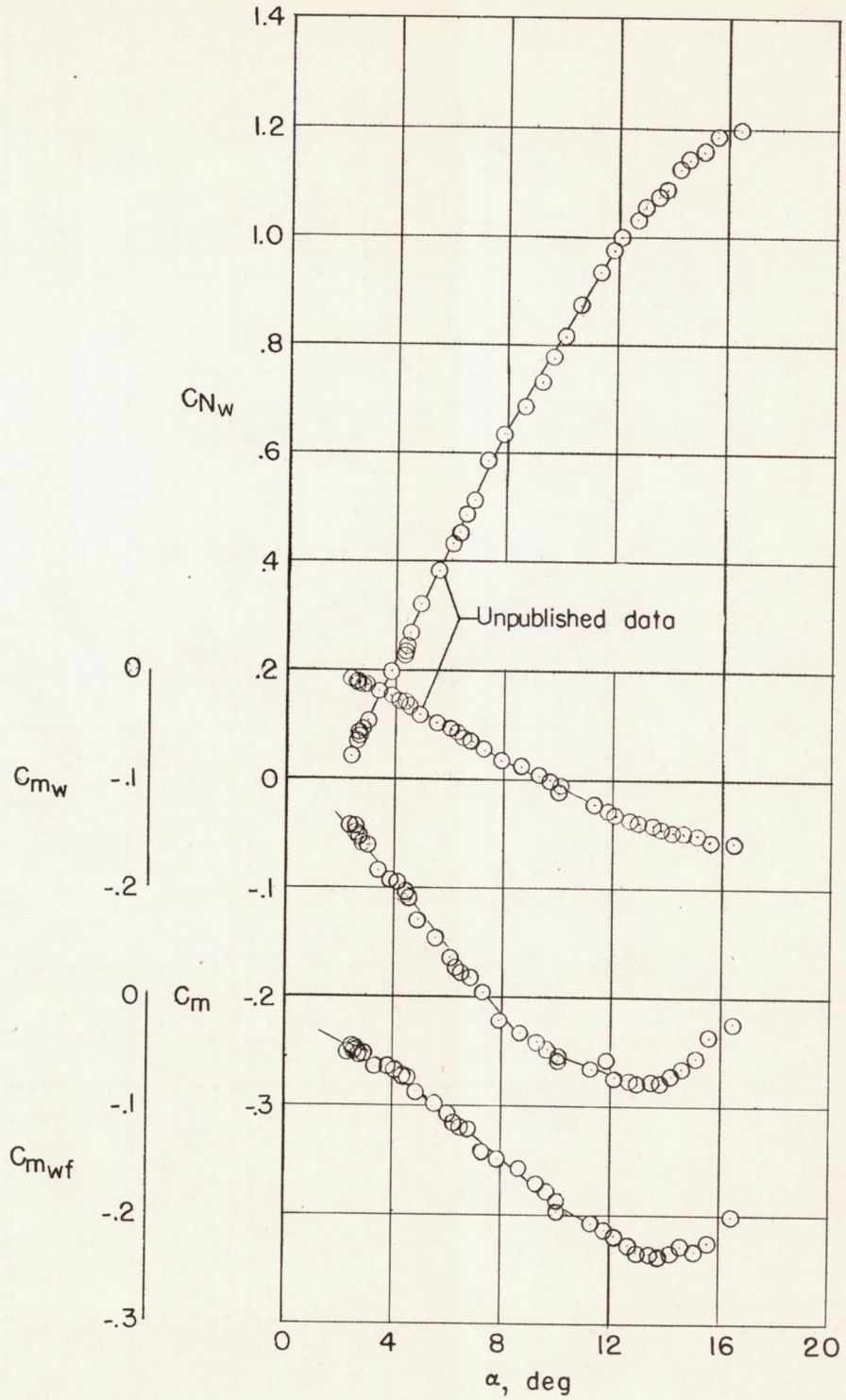

(d) $M \approx 1.10$.

Figure 12.- Concluded.

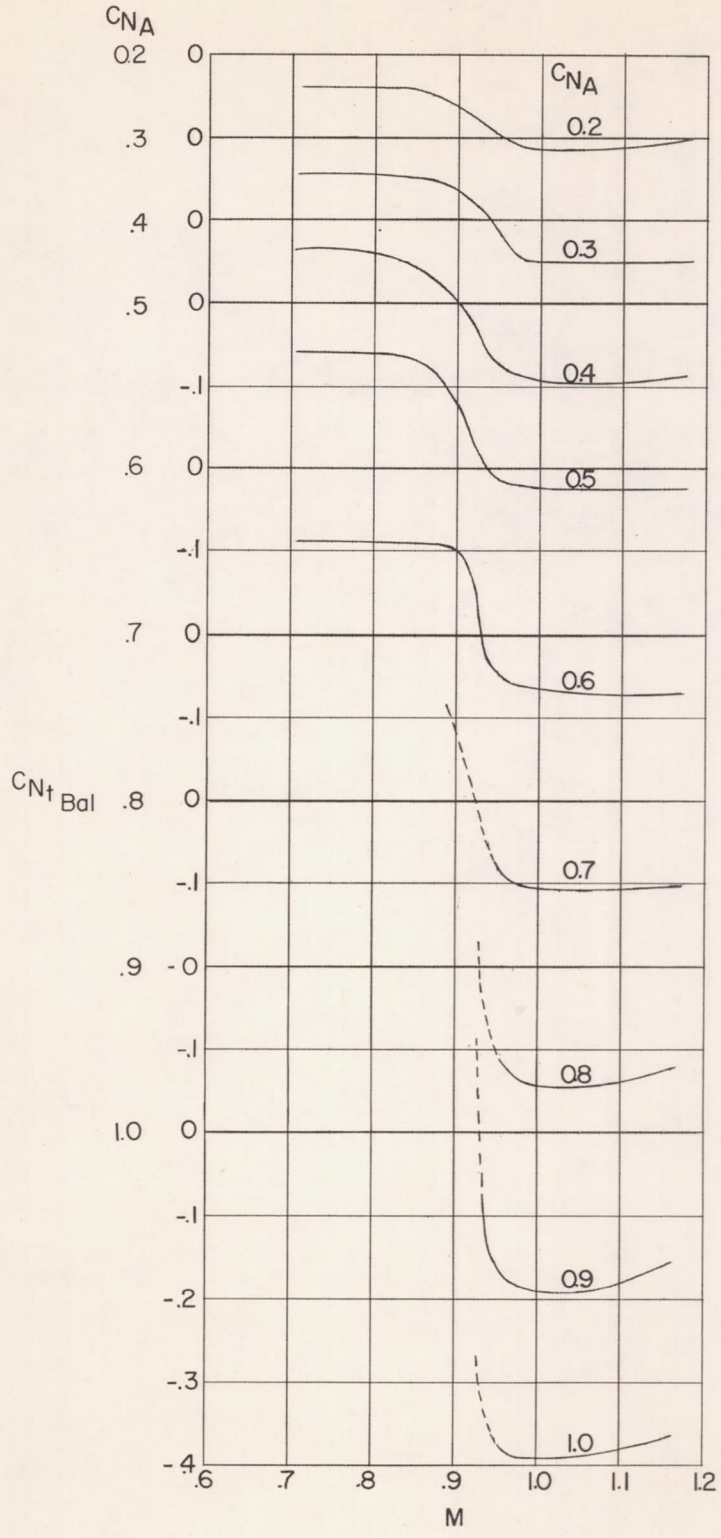

Figure 13.- Variation of balancing-tail-load coefficient with Mach number for various airplane normal-force coefficients.

NACA - Langley Field, Va.